International Journal of Recent Technology and Engineering (IJRTE)
ISSN: 2277-3878 (Online), Volume-8 Issue-4, November 2019

Defect Inspection Based on Segmentation and Defective Tracking in Radiographic Image

C.V.Govindan, D.Jeyasimman, M.Ganesh, R.Narayanasamy

Abstrac: ***In this paper, automatic weld defect segmentation into the radiographic image non-destructive evaluation and testing, with orthogonal polynomials transformation-enhancement (OPT-E) is presented. This proposed system defect identification the given defect Radiographic image. In digital radiographic images, the unknown masses appear very light with weak edges, and hence image enhancement technique needs to be applied with transform domain and radiographic images of some illustrative weld deserts invent. The proposed scheme has three phases. In first phase, a radiographic image enhancement technique, which is performed by logarithmic common variance and enhancement factor, computed from the absolute value of the orthogonal polynomials transformation coefficient as principal parameters for increasing the energy of the masses in the digital radiographic image enhancement. In case of successful enhanced of image in addition to gradient estimation scheme is working to point the edges current, in the next phase. The consequential edge image is again applied with orthogonal polynomials. In the final phase, edge tracking are the salient features with angle based defect identification. Experimental is improved quality of images and high relative segmentation by OPT-E.***

Keywords: ***In digital radiographic images, the unknown masses appear very light with weak edges,***

I. INTRODUCTION

Non-Destructive testing plays an important part in making certain the safe, good, ready doing a play of the joined welded parts. Radiography, Ultrasonic Image, Radiography, and magnetic resonance imaging are the most commonly used NDT techniques. Several research works have been presented on the detailed comparison of these techniques [1-3]. In the current industry trend Gamma Radiography Testing is one among the most important applications of radio-isotopes. This technique is most frequently used in industries to examine the weld quality by analyzing the radiographic image. Compared to other techniques this method of NDT is completely non-invasive rapid and very economical.

Manuscript published on November 30, 2019.
* Correspondence Author
C.V.Govindan*, Department of Mechanical Engineering, Periyar Maniammai University, Thanjavur-613403, Tamil Nadu, India.
D.Jeyasimman, Department of Mechanical Engineering, Periyar Maniammai University, Thanjavur-613403, Tamil Nadu, India.
M.Ganesh, Department of Computer Science Engineering, Shadan College of Engineering & Technology, Hyderabad - 500008, Telangana, India.
R.Narayanasamy,Department of Production Engineering, National Institute of Technology, Tiruchirappalli-620015, Tamil Nadu, India.

Gamma radio isotopes are used in GRT to inspect the materials regarding their defects in the welds in radiographic films. A professional person is necessary to find the defects from the obtained radiographic image. Hence in a situation of non availability of a skilled person, an automatic system is required for defect identification from the radiographic image. An automatic defect detection system generally digitizes the radiographic image enhances the image prior to defect detection [4-9]. In the defect detection in NDT&E the two major problems that possed a challenging design is the low quality of the RT image and algorithms with improper segmentation [10, 11]. The RT image must have enough details and enhanced contrast to obtain a proper result. Progress the quality of the radiographic images many image-processing models are presented that are a basis for defect detection through automatic segmentation [12]. In support of acquiring helpful information starting a low quality digital image enhancement process is traditionally adapted [13-15]. The low contrast is the main constrain that leads for the enhancement of the RT images.

Many useful image processing methods for instance background deduction [16-17], level of gray contour examination [18, 19], texture feature analysis [23], fuzzy reasoning [22], watershed algorithm [21] and mathematical morphology [20], are proposed by researchers all over the world. These techniques use the information available in the digital images and used information from single image for weld defect detection.

The defects in the radiographic weld image are distinguished utilizing well known compel for coordinating and following. There are a couple of concentrates on deformity programmed identification by using the return of defects in grouping of radiographic images to enhance a recognition comes about. For example, The fundamental assignment in on line programmed deformity recognition is currently centered around segmentation and area of distinguishes in weld [24], while the primary undertaking in disconnected defect identification is right now centered around arrangement of various sorts of weld surrenders [25]. Progressively radiographic image succession of a moving weld, it is difficult to recognize the low-differentiate defect, and the false deformity caused by clamor even by human examination if utilizing just a single image. Subsequently, the strategies to distinguish absconds utilizing just a single image each time can't tackle the contention between identifying weld surrenders and staying away from false alerts continuously programmed deformity discovery. At present, there are a couple of concentrates on deformity programmed discovery by using the return of defects in succession of radiographic images to enhance a recognition result.

For example, Mery and Filbert et al. [26] proposed a mechanized blemish recognition strategy in aluminum castings in view of the following of potential defects in a radioscopic image arrangement, and Zhou and Du [27] introduced a robotized deformity location procedure in light of various radiographic images to identify the deformity of the sharp edge of the flight motor. In the two techniques, a grouping of radiographic images are caught from various known places of the work piece, and afterward the potential deformity is coordinated and followed from image to image by a few requirements, for example, epipolar imperative. All things considered, the two techniques have the prerequisites that the imaging framework should be aligned and the position of the protest must be known, and in this manner, they are not appropriate to constant radiographic image grouping of weld whose moving pace is obscure. Du et al. [28] displayed a strategy for enrolment of image grouping by identifying the weld heading and stage connection.

In the technique presented by Jiaxin Shao [29] the defects in the welding radiographic image is identified by weld extraction and defect segmentation where the real defect is identified from regular track in sequence were as the false defects are classified as the one with random appearance. In several applications namely, identification of speaker, detection of land mine, and identification of finger print uses MFCCs along with the polynomial features. These feature exhibit robustness to noise and good quality of time shifts in signals. Hence these techniques are in defect detection even in the noisy environment. In the method proposed by O. Zahran et al.,[30] defect features are obtained using MFCCs and polynomial coefficients that are extracted from the PDSs of the segmented areas of a weld radiographic image. Programmed location of weld defects in a continuous radiographic image for the most part comprises of two stages: (1) weld extraction and (2) deformity segmentation. We exhibit an original thought as the third step for weld defect programmed identification. The thought is to recognize genuine deformities from false defects caused by commotion by following the relative focuses of mass of potential defects in grouping of images. In this work, defect types involve random gradient directions, while the normal grain edges generally present more consistent gradient directions in a small spatial window. It cannot be directly extended to other defect types such as holes that show only line-shaped figures and presented a low variation in gradient directions. While many techniques have been developed to limit the adverse effects of these parameters on image, many of these methods suffer from a range of issues such as computational involvement of algorithms to suppression of useful information. In few image-processing applications, use of transformation has been made effective for edge identification, such as wavelet [31]. Other than surface, edge assumes a huge part in deformity location, particularly to repay or fill the abandoned territory. Great numbers of works are accounted for elite edge extraction. It incorporates Sobel [35], Watchful [34], Roberts [32], and Prewitt [33] administrators. Every one of these administrators are first-arrange subsidiaries. Marr and Hildreth [36] recommended Laplacian, a zero-intersection administrator, as a moment arrange subsidiary, and is utilized to build up the area of edges introduce in the picture. Ganesan and Pritimoy Bhattacharyya [37] announced the location of zero intersections in the second directional subordinates of the picture locale. Utilization of edge in defect distinguishing proof requires cautious investigation and necessities to handle many issues, including non-supression of low level data, and computational cost. Likewise, it can be watched that the greater part of the current deformity recognition plans are accounted for to be application subordinate and no non specific model based framework exists that can be computationally less exorbitant. Subsequently in this paper, a basic computational model for deformity discovery in view of orthogonal polynomials is proposed. The recognized defects are spoken to in a double frame to imagine the identification comes about and to discover exact deformity position, shape, and size. The method of reasoning is that the genuine defect will show up with general track in succession of pictures, while the false deformities coming about because of clamor will show up arbitrarily. Still, there is a great need of efficient weld defect identification scheme that can suit this application. Hence, a simple weld defect identification scheme based on segmentation and edge traces is designed in this communication.

Likewise, it can be watched that the vast majority of the current inadequate district recognizable proof plans are accounted for to be application ward and semi-computerized, requiring contribution from the client. Therefore, in this paper, a computational model for a fully automated defective region identification based on the orthogonal polynomials model is proposed. Orthogonal polynomials is described in section 2. The image enhancement module has been explained in section 3 followed by the edge detection explained in section 4. Boundary tracing is described in section 5. The obtained performance measurement and results and discussions have been reported in section 6, 7 with the conclusions of the system in section 8.

II. MODEL FOR DEFECT SEGMENTATION WITH ORTHOGONAL POLYNOMIALS

The orthogonal polynomials display for the proposed deformity identification and inpainting are introduced In this section. This model is worked with an arrangement of orthogonal polynomials capacities characterized in [34]. From these polynomials which are of degrees 0, 1, 2… n-1, a point spread administrator M of various sizes is built as

$$|M| = \begin{vmatrix} u_0(t_0)\, u_1(t_0) \cdots u_{n-1}(t_0) \\ u_0(t_1)\, u_1(t_1) \cdots u_{n-1}(t_1) \\ \vdots \\ u_0(t_{n-1})\, u_1(t_{n-1}) \cdots u_{n-1}(t_{n-1}) \end{vmatrix}$$

for $n \geq 2$ and $t_i = i$. This operator, that defines linear orthogonal transformation for defect identification can be obtained as $|M| \otimes |M|$, where $|M|$ is computed and scaled to integers as follows.

$$|M| = \begin{vmatrix} 1 & -1 & 1 \\ 1 & 0 & -2 \\ 1 & 1 & 1 \end{vmatrix} \quad (1)$$

The orthogonal polynomials work class of describes the nearby normality of signs by decaying signals into basic building hinders that are all around confined in recurrence plane, and catch the fundamental instrument of traditional edge and texture features. The details on orthogonal polynomials model, with basis functions for purpose of constructing back the original image from transform coefficients can be referred to [31 - 33].

III. IMAGE ENHANCEMENT

In digital radiographic images, the hidden masses appear very light with weak edges, and hence image enhancement technique needs to be applied first. The hidden masses represent either a tumor or a hard tissue, thus an enhancement process can provide improved visual appearance and can set a better way to define the further steps of image processing such as segmentation and feature analysis. In this proposed work, the defected regions in the digital radiographic images were enhanced using an image enhancement algorithm developed with orthogonal polynomial

model. As per our proposed technique, $\beta^{'}$ is the orthogonal polynomial coefficient of the digital
radiographic image with dimensions (n x n) as explained in the previous section.

The proposed anticipated enhancement technique employs the common variance $(\beta_q^{'}(i,j))$, logarithmic common variance $\left(\beta_r^{'}(i,j)\right)$ and enhancement factor (e_f), computed from the absolute value $(\beta_m^{'})$ of the $\beta^{'}$ as principal parameters for increasing the energy of the masses in the digital radiographic image.

We obtain the common variance $\beta_q^{'}(i,j)$ of the absolute value ($\beta_m^{'}$) with the condition that the root α being a non-zero value within 1, and in our application α is set with a constant value. The logarithmic value of the common variant $\beta_r^{'}(i,j)$ of the absolute value ($\beta_m^{'}$) with root γ as a constant value limited between a non-zero value within 2. Two times the entire coefficient is divided by the $\beta^{'}(0,0)$ to assign the enhancement factor (e_f) obtained from equation (2).

$$e_f = {2\times\left(\beta_m^{'}(i,j)\right)} \Big/ {\beta_m^{'}(0,0)} \qquad (2)$$

where $\beta_m^{'}(i,j)$ represents the magnitude of orthogonal polynomial coefficient $\beta^{'}(i,j)$.

The enhanced image $\beta_e^{'}$ with clearly visible defects is obtained by computing the dot product of the predicate value $\beta_p^{'}(i,j)$ along with $\beta^{'}(i,j)$ as per equation (4), where $\beta_p^{'}(i,j)$ is obtained by the sum of enhancement factor and cross product of common variance ($\beta_q^{'}(i,j)$), logarithmic common variance ($\beta_r^{'}(i,j)$) from equation (3).

$$\beta_p^{'}(i,j) = e_f + \beta_q^{'}(i,j)\times\beta_r^{'}(i,j) \qquad (3)$$

$$\beta_e^{'}(i,j) = \beta_p^{'}(i,j)\bullet\beta^{'}(i,j) \qquad (4)$$

Boundaries of the masses in the enhanced digital radiographic image are identified with the proposed edge detection technique in the next section. Boundaries are the markers of different regions within an image that are used for accurate segmentation of Region of Interest (defects) in this application.

IV. EDGE-BASED EXTRACTION FROM ENHANCED RADIOGRAPHIC IMAGES AND DEFECT SEGMENTATION

In this proposed work, the enhanced image under analysis is assumed to have low level features such as edge, texture and uniform background with structural similarities. Presently, to compute an angle, from the orthogonal polynomials show coefficients, we consider only the first-order differences, β'_{01} and β'_{10} and the strength of the gradient Gf_1 are determined as:

$$Gf_1 = (\beta_{01}^{'\,2} + \beta_{10}^{'\,2})^{1/2} \qquad (5)$$

This gradient quality is to be confirmed with a limit τ, for recognition of edges, as their vast esteems having noticeable edges being isolated with little esteems contributing towards almost uniform dim level territory. This plan, when connected to the computerized radiographic, should create a double pictures. The determination of limit τ, is depicted in the accompanying subsection, alongside applicable writing on edge.

V.EDGE TRACKING BASED DEFECT SEGMENTATION

The image obtained in the previous section contains all the strong edges containing both defected and non defected regions. To segment, the defected regions. An edge tracking schema is applied on the edge image $|\beta_{e(i,j)}^{'}|$. This algorithm looks for the looped edge, which is the edge who boundary coordinates begins the ends at the same point giving it a structural perception. The scanning technique is initiated to identify the first edge pixel. Once it identifies the initial edge pixel, it finds for next edge pixel. The orientation of the identified pixels is calculated as per formula 8.

$$\theta_d = \tan^{-1}\left(\frac{j_2 - j_1}{i_2 - i_1}\right) \qquad (6)$$

Where, the tangent of the angle is the ratio of the i_1 -coordinate is difference principal position and i_2 -coordinate of the difference next position to the i_1 -coordinate is difference first position and i_2 -coordinate of the difference subsequent position for the edge parts.

The extraction is looped edges with two parameters, the orientation angle and coordinates matching. Spiral searching [49] is initiated to identify the next edge pixel. If connected edges exist, then the search travels in the forward direction, or else it returns to the first position. Once the connected edges are identified, the boundary coordinates are plotted on the original image for further clinical evaluation. The regions bounding the identified boundaries are set with high values. The pixel counting loop is used to identify the area of the defects present in the high values binary image. Same algorithm is used to calculate the area of the image in pixels from the binary image, obtained from the raw digital radiographic image with minimum threshold value.

VI. EXPERIMENTS AND RESULTS

The proposed radiographic image's deformity recognition framework in light of orthogonal polynomials coefficients, has been explored different avenues regarding more than 150 radiographic pictures of various sorts. The radiographic pictures of some illustrative weld deserts originate from a real turbine result of a heater control hardware fabricating endeavor in K.V.K industry, Tiruchirappalli. Five deformities incorporate porosity, slag, split, inadequate combination (henceforth alluded to be as in-combination), and fragmented infiltration (in the future alluded to be as in-entrance), which are physically isolated from the crude RT pictures. On account of room constraint, just a couple of the example test pictures, their sizes are 135 × 112, 140 × 122, 152 × 143, 205 × 108, and 162 × 67 with pixel esteems in the determination is equivalent to 45 μm are appeared in Fig. 1.

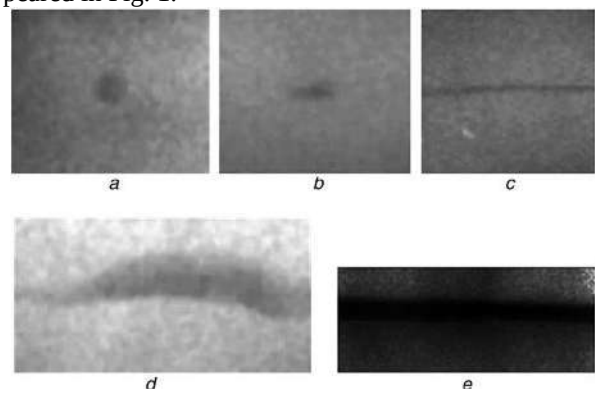

Fig. 1 RT (Radiographic Testing) images with weld defect [14].
(a)Porosity, (b) Slag, (c) Crack, (d) In-fusion, (e) In-penetration.

These unique pictures are at first contaminated with deformities of various shape and size. The surrendered pictures are displayed in Fig. 1. The information deformity pictures are divided into (3 x 3) squares and connected with the orthogonal polynomials show as portrayed in section 2. Relating the orthogonal polynomials demonstrate coefficients and proposed picture upgrade the procedure is completed, as portrayed in section 3. The outcomes acquired with the proposed picture upgrade procedure for the pictures appeared in Figure 2(f). With the subsequent upgraded changed coefficients, we register the edge estimation and get edge removed picture as portrayed in section 4.

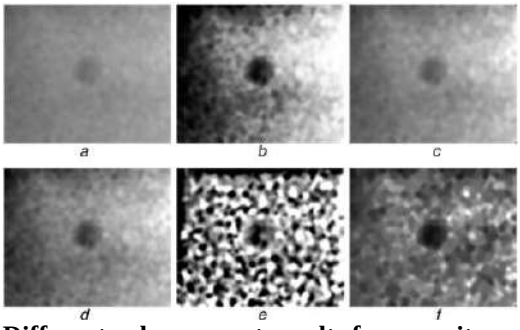

Fig. 2 Different enhancement results for porosity.
(a)ORI, (b) AHE, (c) FEA, (d) GCE, (e) LCE, (f) OPT-E.

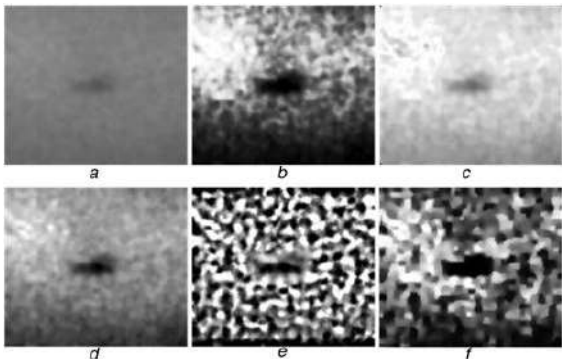

Fig. 3 Different enhancement results for slag.
(a)ORI, (b) AHE, (c) FEA, (d) GCE, (e) LCE, (f) OPT-E.

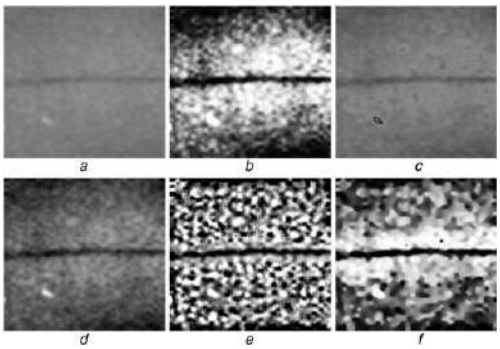

Fig. 4 Different enhancement results for cracks
(a) **ORI, (b) AHE, (c) FEA, (d) GCE, (e) LCE, (f) OPT-E .**

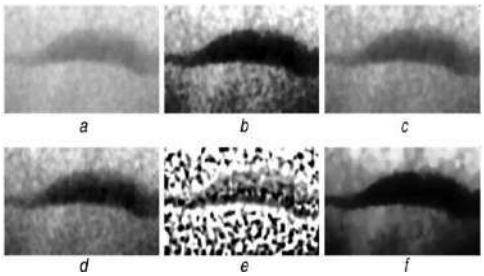

Fig. 5 Different enhancement results for in-fusion
(a)ORI, (b) AHE, (c) FEA, (d) GCE, (e) LCE, (f) OPT-E.

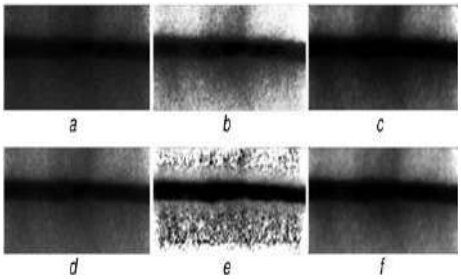

Fig. 6 Different enhancement results for in-penetration (a)ORI, (b) AHE, (c) FEA, (d) GCE, (e) LCE, (f) OPT-E.

From this edge detection image, the regions with looped boundaries can be extracted. The looped boundaries are only regions in the defective which contains the defected area. From this edge detection technique, the edges of noise which don't constitute the defective region can be excluded and only the regions with the looped edges will be segmented. The salient feature of this automated defect detection system is to identify the edges of the defect automatically without the specification of ROI. In order to estimate the region of defects, an edge tracking is initiated. Using the edge orientation and matching the edge coordinates, the edges around the defects are estimated. Defects are looped structures having same initial and terminal point. The algorithm looks for the connectivity of high pixels (values with 255) along the orientation at an angle θ. The boundaries that form a looped structure segment that region as defects as described in Section 4.

The execution of proposed deformity recognition framework with orthogonal polynomials show is additionally contrasted and existing Versatile Histogram Evening out (AHE) [13], Fluffy Improvement Calculation (FEA) [52], Worldwide Differentiation Upgrade (GCE) and Nearby Difference Improvement (LCE) strategies [30], the execution of OPTE is shown by the relative trials of picture quality assessment and defect segmentation of some upgraded pictures. From Figs. 3 a, b, c and d, we can plainly observe that the defect pictures have low complexity, picture obscure, and feeble edges; in this manner, it is hard to recognize and portion the weld surrenders from these low-quality pictures. What's more, an in-infiltration deformity picture with a generally high difference yet low quality is appeared in Fig. 1e. It will be utilized for showing the possibility of a versatile improving normal for OPTE in the resulting tests.

The deformity's unique pictures (ORI) and the pictures upgraded by the diverse improvement calculations are appeared in Figs. 2– 6, separately. Subfigures an of Figs. 2– 6show the first deformity pictures; they are improved by AHE, FEA, GCE, LCE, and OPT-E, as appeared in subfigures b, c, d, e, and f of Figs. 2– 6, individually. From Figs. 2– 6, we can obviously observe that the RT defect pictures were altogether upgraded by AHE and OPT-E. The weld absconds turned out to be clear, in spite of the fact that they displayed obscuring and a low differentiation in the ORI. Notwithstanding, the after effects of FEA, AHE, GCE, and LCE were unacceptable, especially when the first RT picture had a generally low difference or high differentiation. Subjectively, we could plainly observe that LCE decimated the respectability of deformities and neglected to upgrade the RT pictures when the RT pictures have a moderately low difference, picture obscure, and frail edges. Specifically, under-upgrade and over-improvement were seen in the aftereffects of FEA and GCE. In the aftereffects of AHE and LCE, over-improvement was frequently watched. Further, it ought to be noticed that LCE had an outskirt impact.

Table 1 Quality Evaluation Values of the Enhanced Images

No.	Type	Image	ID	IDE	EF	DE
1	porosity	ORI	102.87	1.44	14.93	6.18
		AHE	1658.30	5.80	49.00	5.80
		FEA	424.90	2.63	27.58	6.17
		GCE	640.58	3.65	37.68	6.18
		LCE	1975.50	26.70	26.80	7.10
		OPT-E	1790.70	6.60	57.40	7.50
2	slag	ORI	27.64	0.94	9.26	4.97
		AHE	1684.20	6.70	65.10	4.90
		FEA	208.61	2.58	25.89	4.91
		GCE	518.76	4.12	40.65	4.97
		LCE	2032.90	30.60	284.70	5.60
		OPT-E	1820.60	7.50	69.50	5.80
3	crack	ORI	22.72	1.55	14.54	4.48
		AHE	1663.20	11.00	102.60	4.40
		FEA	211.73	4.51	42.95	4.43
		GCE	284.37	5.56	52.21	4.48
		LCE	1857.6	32.30	290.40	7.40
		OPT-E	1731.10	13.60	126.10	5.10
4	in-fusion	ORI	195.65	1.93	20.56	6.58
		AHE	1672.1	4.50	51.70	5.90
		FEA	488.78	2.89	30.93	6.57
		GCE	880.26	4.13	44.08	6.58
		LCE	2086.10	23.70	243.40	6.30
		OPT-E	1801.00	5.10	52.80	7.50
5	in-penetration	ORI	832.28	5.29	50.51	5.52
		AHE	1678.30	7.60	47.90	5.50
		FEA	835.08	4.54	46.11	5.72
		GCE	832.28	6.29	51.59	5.86
		LCE	2019.00	25.20	181.6	6.60
		OPT-E	1744.90	8.20	54.75	7.37

In addition, to portray the nature of the improved pictures quantitatively, the ID, IDE, EF, and DE estimations of the upgraded pictures were figured, as appeared in Table 1. As appeared in Table 1, the markers of the pictures upgraded by OPT-E enhanced fundamentally. Contrasted with the ORI, the ID, IDE, EF, and DE estimations of OPT-E were enhanced by no less than 114.46, 55.01, 8.39, and 13.84%, separately. Also, the expanded scopes of OPT-E were bigger than those of AHE, FEA, and GCE. The ID estimations of OPT-E were higher by no less than 4.08%, 113.74%, and 104.6% than

those of AHE, FEA, and GCE, separately; the IDE estimations of OPT-E were higher by no less than 7.9%, 96.47%, and 23.49% than those of AHE, FEA, and GCE, individually; the EF estimations of OPT-E were higher by no less than 6.0%, 18.74%, and 6.13% than those of AHE, FEA, and GCE, individually; and the DE estimations of OPT-E were higher by no less than 15.91%, 14.16%, and 13.84% than those of AHE, FEA, and GCE, separately. In spite of the fact that the quality pointers of LCE enhanced radically, LCE neglected to upgrade a low-quality RT picture. Utilizing quality assessment estimations of porosity in Table 2 for instance, contrasted with the first picture, the ID, IDE, EF, and DE estimations of LCE were enhanced by 1820.38%, 1754.17%, 79.50%, and 14.89%, individually. Notwithstanding, from Fig. 2e, we could obviously observe that the uprightness of porosity is demolished by LCE and the neighborhood over-improvement additionally exists. In other words, the LCE calculation

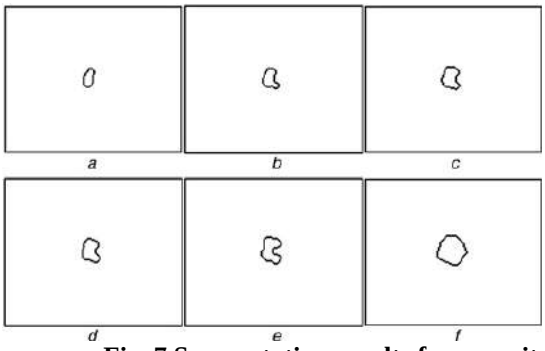

Fig. 7 Segmentation results for porosity (a)ORI, (b) AHE, (c) FEA, (d) GCE, (e) LCE, (f) OPTE .

can't get the acceptable outcome, and the principle reasons are the nearby upgrade normal for LCE and its affectability of clamor. Moreover, other deformity pictures improved by LCE likewise have the wonder like the porosity picture.

Table 2. Average Improvement Range Ratios of Quality Evaluation Values

Method	A_{ID}, %	A_{IDE}, %	A_{EF}, %	A_{DE}, %
AHE	3054.09	333.60	310.30	−3.93
FEA	382.17	94.79	98.28	0.19
GCE	745.02	173.14	169.93	1.21
LCE	3936.90	1810.55	1357.13	23.30
OPT-E	3574.01	442.60	402.63	21.43

Likewise, since we have tried different things with 150 RT pictures, the normal change extend proportions of ID, IDE, EF, and DE estimations of all pictures improved by the diverse upgrade calculations were figured, as appeared in Table 2. In the table, Guide, Associate, AEF, and ADE speak to the normal change go proportions of ID, IDE, EF, and DE estimations of improved pictures contrasted with that of unique RT pictures, separately. As appeared in Table 2, the normal change go proportions of value assessment estimations of OPT-E were higher than those of AHE, FEA, and GCE. Those of LCE were not considered on the grounds that LCE neglected to upgrade the RT pictures.

Since the information pattern of Table 2 was like that of Table 1, the solid examination of them was not to go into points of interest. In synopsis, OPT-E displayed great upgrade comes about and was better than alternate strategies while improving low-quality RT pictures. Further, the improvement level of OPT-E showed a versatile trademark as indicated by the distinctive complexity estimations of the first RT pictures. Since the ID estimation of the first picture of in-infiltration was more prominent than that of alternate deformities, the comparing weighting coefficient a was bigger and the relating improvement degree is littler than those of alternate defects (as appeared in Table 1). Then again, to represent the computational multifaceted nature of OPT-E, we directed an explore different avenues regarding the running time in a PC with Pentium (R) Double Center CPU E6500 at 2.93-GHz and 3-GB of Slam. Every one of the calculations were coded and keep running on java. The picture in the examinations is the radiographic picture of the implantation deformity that is appeared in Fig. 1(d), and it is 205 × 108 pixels in estimate. The normal calculation time of 10 keeps running of AHE, FEA, GCE, LCE, and OPT-E is appeared in Table 3. It can be closed from Table 3 that the computational time of OPT-E was bring down by 74.57% than that of LCE. In any case, the table additionally demonstrates that OPT-E required marginally more computational time than AHE, FEA, and GCE. In the light of the great consequence of OPT-E, the computational time of OPT-E is acknowledged in RT picture preparing and can be lessened by streamlining the calculation bit by bit.

Table 3 Computational time of the different enhancement algorithms

Type	**AHE**	**FEA**	**GCE**	**LCE**	OPT-E
Time (s)	0.032	0.112	0.025	2.458	0.625

A. Defect Segmentation of Enhanced Images

To additionally consider the impact of the proposed OPT-E with edge recognition and following on defect segmentation, a district developing segmentation is performed. Specifically, its key focuses were the choice of the developing seed and the district developing criteria [51]. To think about the segmentation comes about between OPT-E and AHE, FEA, GCE, and LCE, we guaranteed that the developing seed was the same for each kind of deformities and the end edge was the same for a wide range of defects. The improved picture was standardized before the district developing segmentation, and the end edge was 0.059. The segmentation aftereffects of the deformity pictures upgraded by the diverse improvement calculations are appeared in Figs. 7– 11, individually. Subfigures of Figs. 7– 11 demonstrate the segmentation consequences of the first deformity pictures. Subfigures b, c, d, e, and f of Figs. 7– 11 demonstrate the segmentation aftereffects of the defect pictures improved by AHE, FEA, GCE, LCE, and OPT-E, separately. In Figs. 7– 11, differential edges were seen in the defect segmentation comes about. Clearly, the segmentation trustworthiness and exactness of the defects were fundamentally enhanced by the proposed OPT-E with edge identification and following. Subjectively, the pictures improved by OPT-E had a higher segmentation execution than the pictures upgraded by AHE, FEA, GCE, and LCE.

Also, the over-segmentation saw in Fig. 11c could be credited to the over-improvement of FEA. As a result of the under-improvement, under-segmentation existed in the majority of the upgraded pictures aside from the pictures upgraded by OPT-E with edge discovery and following.

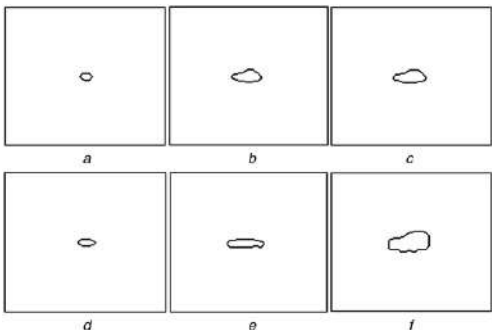

Fig. 8 Segmentation results for slag (a)ORI, (b) AHE, (c) FEA, (d) GCE, (e) LCE, (f) OPT-E.

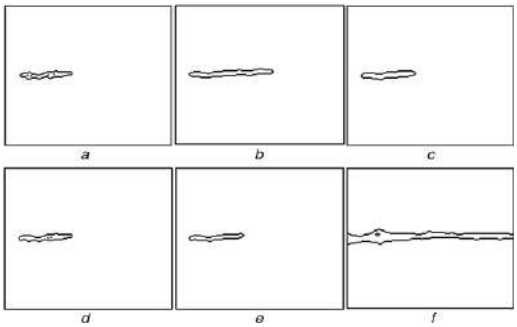

Fig. 9 Segmentation results for cracks (a)ORI, (b) AHE, (c) FEA, (d) GCE, (e) LCE, (f) OPT-E.

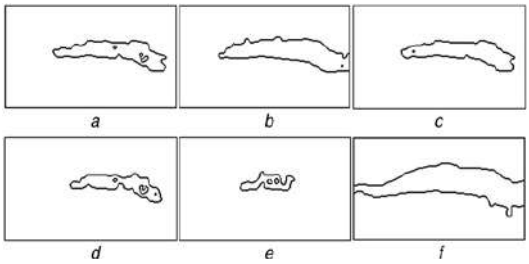

Fig. 10 Segmentation results for in-fusion (a)ORI, (b) AHE, (c) FEA, (d) GCE, (e) LCE, (f) OPT-E.

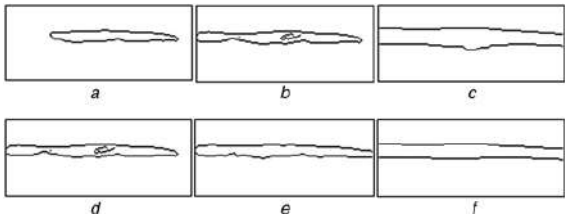

Fig. 11 Segmentation results for in-penetration (a)ORI, (b) AHE, (c) FEA, (d) GCE, (e) LCE, (f) OPT-E.

The quantitative assessments of the defect segmentation comes about are appeared in Table 4. In the table, RSA1 indicates the RSA of the first RT pictures. RSA1, RSA2, RSA3, RSA4, and RSA5 speak to the relative segmentation correctnesses of the pictures upgraded by AHE, FEA, GCE, LCE, and OPT-E with edge recognition and following, individually. From Table 4, we deduce that the RSA enhanced surprisingly. The utilization of the proposed OPT-E enhanced the RSA of porosity from 31.89 to 95.92%, that of slag from 19.42 to 98.68%, that of split from 30.97 to 97.27%, that of in-combination from 52.84 to 99.44%, and that of in-infiltration from 57.02 to 98.39%. What's more, the relative segmentation correctnesses enhanced by the utilization of AHE, FEA, GCE, and LCE; be that as it may, the change scopes of these strategies were lower than the change scope of OPT-E. Likewise, since we have explored different avenues regarding 100 RT pictures, the normal RSA estimations of upgraded pictures by AHE, FEA, GCE, LCE, and OPT-E are 58.45%, 59.60%, 50.39%, 48.44%, and 96.47%, individually. All the more particularly, the proposed OPT-E can radically enhance RSA esteem and has the most noteworthy normal RSA esteem. In the wake of investigating countless consequences of 100 test pictures, we can solidly express that the proposed OPT-E has higher RSA of over 95%. This estimation of 95% is the insignificant incentive in all the segmentation aftereffects of various deformities. In rundown, the trial comes about demonstrate that the proposed calculation has a decent picture upgrade impact as well as an exceptionally useful effect on RT defect segmentation.

VII. CONCLUSION

OPT-E complying with weld defect segmentation is proposed and shown in this paper. Joining OPT-E, we deliberately improved a unique RT picture; in the interim, the necessity of defect segmentation was considered. Henceforth, we could explain the clashing issues of clamor intensification, picture obscure, edge misfortune, over-upgrade, and under-improvement, which regularly exist in traditional improvement with edge recognition and following. The near trial comes about demonstrated that the proposed calculation could fundamentally enhance the picture quality and segmentation precision. Further, it defeated the downsides of utilizing improvement and protected more helpful picture edges and points of interest while upgrading a picture. Countless with various RT defect pictures demonstrated that the proposed OPT-E is powerful and has the all inclusive statement of utilization to low-quality RT pictures. Consequently, it is extremely helpful for upgrading low-quality RT pictures and enhancing the precision of programmed defect segmentation in mechanical NDT&E. The performance of the proposed scheme is computed with standard measures and found to give better results when compared to other existing schemes.

REFERENCES

1. Zahran O, Al-Nuaimy W. Recent development in ultrasonic techniques for rail-track inspection. In: Proceedings of NDT2002 Conference, UK; 2002. 55–60.
2. Ditchburn RJ, Burke SK, Scala CM. NDT of welds: state of the art. NDT E Int 1996;29(2):111–7.
3. Charles Hayes. The ABC's of non destructive weld examination. Weld J 1998;76(5):46–51.
4. Liao TW, Ni J. An automated radiography NDT system for weld inspection: Part II. Flaw Detection. NDT E Int 1998;31(3):183–92.
5. Wang G, Liao TW. Automatic identification of different types of welding defects in radiography images. NDT E Int 2002;35:519–28.

6. Da Silva Romeu R, Siqueira Marcio HS, Vieira de Souza Marcos Paulo, Rebello Joa\widetildeo MA, Calo\widehatb Luiz P. Estimated accuracy of classification of defects detected in welded joints by radiography tests. NDT E Int 2005;38:335–43.
7. Saravanan T, Bagavathiappan S, Philip J, Jayakumar T, Raj B. Segmentation of defects from radiography images by the histogram concavity threshold method. Insight 2007;49(10):578–84.
8. Silva RR, Mery D. State-of-the-art of weld seam inspection by radiography testing: Part I: image processing. Mater Eval 2007;65(6):643–7.
9. Kasban H, Zahran O, Arafa H, El-Kordy M, Elaraby Sayed MS, Abd El-Samie FE. Welding defect detection from radiographic image using cepstral approach. NDT E Int 2011;44(2):226–31.
10. Da Silva, R.R., Mery, D.: State-of-the-Art of weld seam inspection by radiographic testing: part I–image processing, E-J. Nondestruct. Test. Ultrason., 2007, 12, pp. 1–9
11. Shen, Q.M., Gao, J.M., Li, C.: 'Adaptive segmentation of weld defects based on flooding', Insight, 2009, 51, (10), pp. 541–547.
12. Dang, C.Y., Gao, J.M.,Wang, Z., et al.: 'Self-adaptive characteristics segmentation optimized algorithm of weld defects based on flooding'. Proc. Int. Conf. Defense, Security, and Sensing, Baltimore, USA, April 2013, vol. 8745.
13. Nacereddine, N., Zelmat,M., Belaifa, S.S., et al.: 'Weld defect detection in industrial radiography based digital image processing'. Proc. Int. Conf. World Academy of Science Engineering and Technology, Berlin, Germany, January 2005, pp. 112–115
14. Rathod, V.R., Anand, R.S.: 'A comparative evaluation of different segmentation techniques to detect flaws in weldments radiographically', Insight, 2011, 53, (10), pp. 542–551.
15. Kasban, H., Zahran, O., Arafa, H., et al.: 'Quantitative and qualitative evaluation for gamma radiographic image enhancement', Int. J. Signal Process. Image Process. Pattern Recogn., 2012, 5, (2), pp. 73–88 10
16. Mu, W.L., Gao, J.M., Chen, F.M., et al.: 'Weld radiographic image enhancement conforming to Human visual system', J. Xi'an Jiaotong Univer., 2012, 46, (3), pp. 90–93.
17. Kaftandjian V, Dupuis O, Babot D, Zhu YM. Uncertainty modelling using Dempster–Shafer theory for improving detection of weld defects. Pattern Recogn Lett 2003;24:547–64
18. Liao TW, Li YM. An automated radiographic NDT system for weld inspection: Part II—flaw detection. NDT&E Int 1998;31:183–92.
19. Padua GX, Silva RR, Siqueira MHS, Rebello JMA, Caloba LP. Classification of welding defects in radiographs using transversal profiles to the weld seam. In: 16th world conference on nodestructive testing.
20. Lawson SW. Automatic defect detection in industrial radioscopic and ultra- sonic images. London: University of Surrey; 1996.
21. Alaknanda Anand RS, Kumar P. Flaw detection in radiographic weldment images using morphological watershed segmentation technique. NDT&E Int 2009;42:2–8.
22. Lashkia V. Defect detection in X-ray images using fuzzy reasoning. Image Vis Comput 2001;19:261–9.
23. Sun Y, Peng B, Sun HY, Zhou P. Real-time automatic detection of weld defects in steel pipe. NDT&E Int 2005;38:522–8.
24. Liao TW. Improving the accuracy of computer-aided radiographic weld inspection by feature selection. NDT&E Int 2009;42:229–39.
25. Mery D, Berti MA. Automatic detection of welding defects using texture features. Insight 2003;45:676–81.
26. Mery D, Filbert D. Automated flaw detection in aluminum castings based on the tracking of potential defects in a radioscopic image sequence. IEEE Trans Robotic Autom 2002;18:890–901.
27. Zhou ZG, Du YY. Automated defects recognition technique based on multiple radiographic images. Chin J Mech Eng 2006;42:73–6.
28. Du D, Hou RS, Shao JX, Chang BH, Wang L. Registration of real-time X-ray image sequences for weld inspection. Nondestruct Test Eval 2010;25:153–9.
29. Jiaxin Shao, Dong Du, Baohua Chang and Han Shi," Automatic weld defect detection based on potential defect tracking in real-time radiographic image sequence", DT&E International 46 (2012) 14–21.
30. O. Zahran, H. Kasban, M. El-Kordy, F.E and Abd El-Samie, "Automatic weld defect identification from radiographic images", NDT&E International 57 (2013) 26–35.
31. W. Sun, A. Romagnoli, J. W. Tringe, S. E. Létant, P. Stroeve and A. Palazoglu, "Line-Edge Detection and Characterization in SEM Images using Wavelets", IEEE Transactions on Semiconductor Manufacturing, Vol. 22, 180-187, 2009.
32. Roberts, L.G, "Machine perception of three dimensional solids", Optical and Electro optical Information processing, MIT Press, Cambridge, MA, 1965.
33. Prewitt, J.M., "Object enhancement and extraction", Image Processing and Psychopictorics, Academic Press, New York, 1970.
34. Canny J, "A computational approach to edge detection", IEEE Trans. Pattern Anal. Machine Intell. Vol. 8 , pp. 679–698, 1986.
35. Sobel, I.E. "Camera models and machine perception", Ph.D. Thesis, Stanford University, 1970.
36. [36] Marr D and Hildreth E.C, "Theory of edge detection", Proc. Roy. Soc., London B 207, pp.187–217, 1980.
37. L. Ganesan and Pritimoy Bhattacharyya , "An orthogonal polynomials based framework for edge detection in 2-D monochrome images," Pattern Recognition, Vol. 18, No.4, pp. 319-333, 1997.
38. R. Krishnamoorthy, "Transform Coding of Monochrome Images with Statistical Design of Experiments Approach to Separate Noise", Pattern Recognition Letters, Vol. 28, No. 7, pp. 771-777, 2007.
39. R. Krishnamoorthy and N. Kannan, "A new integer image coding technique based on orthogonal polynomials" on International journal of Image and segmentation computing – Vol.27, No.8, pp.999-1006, 2009.
40. R. Krishnamoorthy and J. Kalpana, "Generalized Adaptive Bayesian Relevance Feedback in the Orthogonal Polynomials Domain", Signal Processing. Vol.92, No.12, pp.3062-3067, 2012.
41. Otsu, N., "A Threshold Selection Method from Gray-Level Histograms," IEEE Transactions on Systems, Man, and Cybernetics, Vol. 9, No. 1, pp. 62-66, 1979.
42. Kittler, J., Illingworth, J and Foglein, J, "Threshold selection based on a simple image statistic", Computer Vision, Graphics and Image Processing, Vol. 30, pp.125–147, 1985.
43. A. S. Abutaleb, "Automatic thresholding of grey-level images using two-dimensional entropy," Computer Vision, Graphics, and Image Proc., Vol.47, pp. 22–32, 1989.
44. Mehmet Sezgin and Bulent Sankur, "Survey over image thresholding techniques and quantitative performance evaluation," Journal of Electronic Imaging Vol.13, pp. 146–165, 2004.
45. E.R. Davies, "Efficient transformation for identifying global valley locations in 1D data", Electronics Letters, Vol. 43, No.6, pp. 332-333, 2007.
46. Nicolas Coudray, Jean-Luc Buessler, and Jean-Philippe Urban., " Robust threshold estimation for images with unimodal histograms ", Pattern Recognition Letters, Vol. 31, No.9, pp.1010-1019, 2010.
47. R Medina-Carnicer, R. Muñoz-Salinas, A. Carmona-Poyato and F.J. Madrid-Cuevas, "A novel histogram transformation to improve the performance of thresholding methods in edge detection", Pattern Recognition Letters, Vol. 32, No. 5, pp. 676-693, 2011.
48. Ian Hannah, Devesh Patel and Roy Davies, "The use of variance and entropic thresholding methods for image segmentation", Pattern Recognition ,Vol. 28, pp. 1135–1143, 1995.
49. Krishnamoorthy.R, Ganesh.M, "Texture synthesis using spiral algorithm with orthogonal polynomials model" International Conference on Emerging Trends in Science, Engineering and Technology (INCOSET), (2012), pp. 287 – 293.
50. Kasban, H., Zahran, O., Arafa, H., et al.: 'Quantitative and qualitative evaluation for gamma radiographic image enhancement', Int. J. Signal Process. Image Process. Pattern Recogn., 2012, 5, (2), pp. 73–88.
51. Tian, Y., Zhu, M.: 'Study on no-reference quality assessment method for gray image' PhD thesis, Changchun Institute of Optics, Fine Mechanics and Physics, Chinese Academy of Sciences, 2010.
52. Sheeba Jenifer, S. Parasuraman, Amudha Kadirvelu: Contrast enhancement and brightness preserving of digital mammograms using fuzzy clipped contrast-limited adaptive histogram equalization algorithm. Appl. Soft Comput. 42: 167-177 (2016)

AUTHORS PROFILE

C.V.Govindan, doing as a Research Scholar in Mechanical Engineering at Periyar Maniammai University, Vallam, Thanjavur, Tamilnadu.I have completed B.Tech in Production Engineering during April 2004 at Anna University,Chennai and M-Tech in Industrial Engineering during April 2013 at Dr. MGR Educational and Research University, Chennai.At present, I am working as WORKS MANAGER in Integral Coach Factory, Indian Railways, Chennai-38, Tamilnadu.

Dr. D. Jeyasimman working as a Associate Professor and Head of Department in the Department of Mechanical Engineering, Periyar Maniammai Institute of Science & Technology, Thanjavur, Tamil Nadu, India. He has completed his Full Time Ph.D. research work in nanocomposites area. He has more than 20 good publications in international journals (with high impact factors) and thirteen years teaching experience in various engineering colleges & Universities. He has obtained his postgraduate degree in Manufacturing Engineering in Anna University, Chennai, India. He has obtained his undergraduate degree in Mechanical Engineering in Bharathiyar University, Coimbatore, Tamil Nadu, India.

Dr.M.Ganesh is Professor of Department of computer science and engineering at Shadan College of engineering and technology, Hyderabad, India. with over 20 years of teaching and research experience. He has published more than 30 papers in International Journals and made 10 International conference presentationsHis areas of specializations are Image Processing, Computer graphics and signal processing .

Dr.R.Narayanasamy is Professor of Department of Production Engineering at NIT, Tiruchirappalli with over 40 years of teaching and research experience. He has published more than 200 papers in International Journals and made 40 International conference presentations. He completed many research based projects and consultancy works getting funds from various agencies. His areas of specializations are Metal Forming and Powder Metallurgy.